Interplay of exciton coupling and large-amplitude motions in the vibrational circular dichroism spectrum of dehydroquinidine

Nicu, V.P.; Domingos, S.R.; Strudwick, B.H.; Brouwer, A.M.; Buma, W.J.

DOI
10.1002/chem.201503250

Publication date
2015

Document Version
Final published version

Published in
Chemistry: A European Journal

ChemPubSoc Europe

DOI: 10.1002/chem.201503250

CHEMISTRY
A European Journal
Full Paper

Vibrational Circular Dichroism

Interplay of Exciton Coupling and Large-Amplitude Motions in the Vibrational Circular Dichroism Spectrum of Dehydroquinidine

Valentin P. Nicu,*[a] Sérgio R. Domingos,[b, c] Benjamin H. Strudwick,[b] Albert M. Brouwer,[b] and Wybren J. Buma[b]

Abstract: A detailed analysis of the computed structure, energies, vibrational absorption (VA) and circular dichroism (VCD) spectra of 30 low-energy conformers of dehydroquinidine reveals the existence of families of pseudo-conformers, the structures of which differ mostly in the orientation of a single O–H bond. The pseudo-conformers in a family are separated by very small energy barriers (i.e., 1.0 kcal mol^{-1} or smaller) and have very different VCD spectra. First, we demonstrate the unreliable character of the Boltzmann factors predicted with DFT. Then, we show that the large differences observed between the VCD spectra of the pseudo-conformers in a family are caused by large-amplitude motions involving the O–H bond, which trigger the appearance/disappearance of strong VCD exciton-coupling bands in the fingerprint region. This interplay between exciton coupling and large-amplitude-motion phenomena demonstrates that when dealing with flexible molecules with polar bonds, vibrational averaging of VCD spectra should not be neglected. In this regard, the dehydroquinidine molecule considered here is expected to be a typical example and not the exception to the rule.

1. Introduction

Cinchona alkaloid compounds are found in the bark of the various *Cinchona* trees that are native to the eastern slopes of the Amazonian area of the Andes. Apart from their long known medicinal uses, in particular as anti-malaria drugs, cinchona alkaloids and their countless chemically synthesised derivatives have a strong history in asymmetric organocatalysis. These chiral compounds have extraordinary molecular recognition capabilities and as such are often used as chiral modifiers,[1–3] ligands[4,5] or catalysts[6–8] in many stereoselective reactions in organic chemistry.

The conformational landscape of the various cinchona alkaloids compounds has been investigated intensively over the years[9–17] as it has an important influence on the outcome of an asymmetric reaction. Illustrative studies in this respect are: 1) the first investigations performed on cinchonidine and its derivatives by Dijkstra et al.[9,10] and Matsson et al.[11,12] by using nuclear magnetic resonance (NMR), X-ray crystallography and electronic circular dichroism (ECD) techniques, and 2) the more recent studies conducted by Baiker and co-workers[13–16] by using NMR Overhauser enhancement spectroscopy (NOESY), vibrational absorption (VA) and circular dichroism (VCD) spectroscopy, and quantum mechanical calculations based on density functional theory (DFT).

In this work, we present a combined computational–experimental VA and VCD study of the dehydroquinidine molecule (shown in Figure 1). The main motivation for this study is the somewhat contradictory findings reported in two of the most important VCD studies on cinchona alkaloids, that is, the VCD investigation of cinchonidine presented by Burgi et al. in reference [14] and the VCD study of quinidine presented by Sen et al. in reference [18]. On the one hand, both these studies report the presence of a single dominant conformer in the experimental sample, the so-called Open(3) conformer.[14–16,18] As cinchonidine and quinidine have very similar structures, this is not surprising. Visual inspection of the experimental and simulated VCD spectra, on the other hand, finds quite a different level of agreement between these spectra. Reference [14] reports a rather good agreement between the experimental and simulated VCD spectra for the entire fingerprint region (i.e., between 1150 and 1650 cm^{-1}), whereas in reference [18], a good agreement between the experimental and simulated VCD spectra is obtained only for the bands between 1400 and 1650 cm^{-1}.

Our preliminary VCD investigation of the dehydroquinidine molecule has yielded results that are similar to those reported in reference [18], that is, suboptimal agreement between cal-

[a] *Dr. V. P. Nicu*
Theoretical Chemistry, Vrije Universiteit Amsterdam
De Boelelaan 1083, 1081 HV Amsterdam (The Netherlands)
E-mail: V.P.Nicu@uva.nl

[b] *Dr. S. R. Domingos, M. Sc. B. H. Strudwick, Prof. Dr. A. M. Brouwer, Prof. Dr. W. J. Buma*
Van 't Hoff Institute for Molecular Sciences, University of Amsterdam
Science Park 904, XH Amsterdam (The Netherlands)

[c] *Dr. S. R. Domingos*
Current address: Max Planck Institute for the Structure and Dynamics of Matter at the Center for Free-Electron Laser Science and The Hamburg Centre for Ultrafast Imaging, Universität Hamburg, Luruper Chaussee 149, 22671 Hamburg (Germany)

Supporting information for this article is available on the WWW under http://dx.doi.org/10.1002/chem.201503250.

culation and experiment below 1400 cm^{-1} and good agreement between 1400 and 1650 cm^{-1}. This has prompted us to analyse in detail two sources of errors that are expected to affect the computed VCD spectra significantly: the accuracy of the predicted Boltzmann factors and the effects induced in the VCD spectra by large-amplitude motions. As will be shown, both these perturbations induce important changes in the VCD spectra, and, as such, should not be neglected. The high sensitivity of the predicted Boltzmann factors on the level of theory used in calculations is indeed an important source of errors, viz., simulated VCD spectra (obtained as Boltzmann averages over the conformers considered) computed at different levels of theory are very different. Further, the large-amplitude motions involving the O–H bond at the chiral centre trigger the appearance/disappearance of very intense VCD exciton-coupling bands in the fingerprint region.

This interplay between large-amplitude motion and exciton-coupling mechanisms seems to be the main reason for the discrepancy observed between the VCD studies on cinchonidine and quinidine. The strong exciton-coupling VCD bands are triggered by coupling of the transition dipole moments associated with the O–H and C–O bonds, and, as such, cannot occur in cinchonidine, which has no substituent on the quinoline and, thus, lacks the OCH_3 group. Besides providing a clear explanation for the contradictory observation mentioned above, this study provides further evidence[19–21] for the need to perform vibrational averaging of VCD spectra.

2. Molecular Structure

A schematic representation of the dehydroquinidine (DHQD) molecule used as the example in this study is shown in Figure 1. As can be seen, the DHQD molecule consists of two rigid moieties, an aromatic quinoline ring and an aliphatic quinuclidine ring connected by a sp^3 hydroxilated carbon atom.

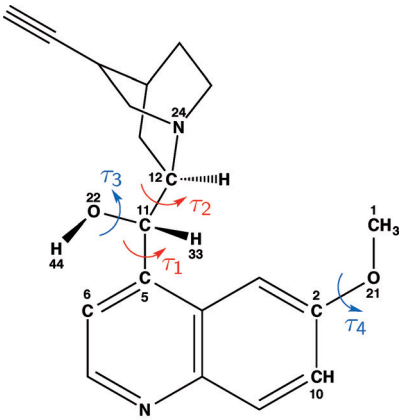

τ_1: $C^6–C^5–C^{11}–C^{12}$

τ_2: $C^5–C^{11}–C^{12}–N^{24}$

τ_3: $H^{33}–C^{11}–O^{22}–H^{44}$

τ_4: $C^1–O^{21}–C^2–C^{10}$

Figure 1. Schematic representation of DHQD. The four dihedral angles (i.e., τ_1, τ_2, τ_3 and τ_4) describing the various conformers of DHQD are indicated and defined.

The various conformers of DHQD can be described by using the four dihedral angles defined in Figure 1, that is, τ_1, τ_2, τ_3 and τ_4. The dihedral angles τ_1 and τ_2 describe the relative orientation of the main quinoline and quinuclidine groups, respectively, whereas τ_3 and τ_4 describe the orientations of the OH and OCH_3 groups, respectively.

The nomenclature and naming convention of the conformers is well established[9,12,13,17] and based on two primary conformations: *Open* and *Closed*, and two additional secondary conformations: *Syn* and *Anti*. The *Open* and *Closed* conformations are determined by the τ_2 dihedral angle (i.e., rotations around the $C^{11}–C^{12}$ bond). In the *Open* conformation, the lone pair of the quinuclidine nitrogen points away from the quinoline ring, whereas in the *Closed* conformation there is an interaction between the quinuclidine nitrogen lone pair and the aromatic π-electron system.

The *Anti* and *Syn* conformers are defined by the rotation of the quinoline moiety around the bond $C^5–C^{11}$ (i.e., by the τ_1 dihedral angle). In the *Anti* orientation, the OCH_3 and quinuclidine moieties are situated on the same side, whereas in the *Syn* orientation the two moieties are situated on opposite sides. It should be noted, though, that the *Syn–Anti* nomenclature becomes ambiguous when τ_1 is close to 90°.

When using the standard naming convention[9,12,13,17] described above, the conformers can be grouped into four different families: *Anti–Open*, *Syn–Open*, *Anti–Closed* and *Syn–Closed*. As will be discussed in Section 3.1, the conformers in a family can be further classified into: 1) subfamilies characterised by similar values for τ_1 and τ_2, and 2) *cis* and *trans* pairs[18] (with respect to the $C^5–C^{11}$ bond) comprising conformers that differ only in the orientations of the OCH_3 group, that is, $\tau_4 = 0°$ versus $\tau_4 = 180°$, and 3) pairs of pseudo-conformers containing conformers that differ only in the orientation of the O–H bond (i.e., have different τ_3 angles).

3. Results and Discussion

3.1. Structural analysis of the predicted conformers

A molecular mechanics conformational search yielded 30 conformers, which have been further re-optimised by using DFT at six different levels of theory, that is, Vacuum/BP86, COSMO/BP86, Vacuum/OLYP, COSMO/OLYP, Vacuum/B3LYP and COSMO/B3LYP. As the structures predicted by these six sets of DFT calculations are very similar (see Section 1.3 in the Supporting Information) only the results obtained from the COSMO/BP86 calculations (our reference calculations) will be discussed here. Table 1 lists the COSMO/BP86 values for the τ_1, τ_2, τ_3 and τ_4 dihedral angles. Table 1 also indicates how the 30 conformers can be distributed into families (column 7), subfamilies (column 6), *cis* and *trans* pairs (column 5) and pseudo-conformer pairs (column 4). The conformers that exhibit an intramolecular hydrogen-bond between the O–H bond and the N atom number 24 are indicated in Table 1 by a star (column 1).

As can be seen, the *Anti–Open* and *Syn–Open* families contain nine conformers each (entries 1–9 and 10–18, respective-

Table 1. Values computed at the BP86/TZP/COSMO levels of theory for the dihedral angles τ_1, τ_2, τ_3 and τ_4. Definitions of dihedral angles: $\tau_1 = C^6\text{-}C^5\text{-}C^{11}\text{-}C^{12}$, $\tau_2 = C^5\text{-}C^{11}\text{-}C^{12}\text{-}N^{24}$, $\tau_3 = H^{33}\text{-}C^{11}\text{-}O^{22}\text{-}H^{44}$ and $\tau_4 = C^1\text{-}O^{21}\text{-}C^2\text{-}C^{10}$. The conformers highlighted in column 1 by a star exhibit an intramolecular hydrogen-bond between the O–H bond and the N atom number 24.

BP86, TZP, COSMO calculations						
Conf.	τ_1	τ_2	τ_3	τ_4	Subfamily	Family
1	−102.9	−163.5	+33.8	−0.7	I	Anti-Open
2	−101.5	−161.5	+36.2	−180.0		
3	−99.8	−158.1	−56.9	−0.8		
4	−99.0	−156.9	−56.0	+179.7		
5*	+84.2	+91.2	+137.2	+1.2	II	
6*	+81.3	+93.8	+134.9	+179.3		
7	+100.5	+58.1	−75.1	+0.1	III	
8	+100.7	+57.8	−75.7	+179.8		
9	−8.3	−154.7	−166.6	−178.7	IV	
10*	−99.7	+92.4	+135.2	−1.6	V	Syn-Open
11*	−99.4	+92.2	+135.1	−179.5		
12	−80.8	+57.2	−72.3	−2.9	VI	
13	−80.8	+55.4	−73.3	−179.1		
14	+85.9	−159.7	+31.6	+0.7	VII	
15	+84.8	−160.7	+31.7	+178.8		
16	+93.4	−147.1	−62.1	+0.1		
17	+92.6	−146.2	−62.8	+179.7		
18*	−4.6	+90.2	+138.2	−177.8	VIII	
19	−4.7	−63.0	−164.0	−3.4	IX	Anti-Closed
20	−5.9	−61.8	−159.9	−177.9		
21	−7.2	−63.1	+54.8	−2.8		
22	−6.0	−63.2	+59.3	−178.4		
23	−53.5	−57.8	−66.3	−1.9	X	
24	−60.6	−59.9	−70.1	−179.3		
25	−64.9	−62.0	+56.9	−1.8		
26	−67.6	−64.0	+59.9	−179.1		
27	+110.1	−60.7	−68.3	−0.3	XI	Syn-Closed
28	+109.3	−58.5	−68.2	+179.9		
29	+109.7	−59.7	+54.1	+0.0		
30	+107.6	−59.6	+56.8	+179.7		

ly), the *Anti–Closed* family contains eight conformers (19–26), and the *Syn–Closed* family contains only four conformers (27–30). The conformers in a given family can be grouped further into subfamilies, with the conformers in a given subfamily having very similar values for the τ_1 and τ_2 angles and different values for the τ_3 and τ_4 angles. In total there are eleven subfamilies (labelled as I–XI): five subfamilies each comprising four conformers (i.e., I, VII, IX, X and XI), four subfamilies each consisting of two conformers (i.e., II, III, V and VI), and two subfamilies consisting of one conformer each (i.e., IV and VIII). To easily differentiate the conformers in the various subfamilies in Table 1, the values of τ_1 and τ_2 angles (which define a given subfamily) have been highlighted in blue and red alternatively.

It is important to mention the similarity between the results obtained here and the results reported by Urakawa et al. in reference [16]. By using the cinchonidine molecule (which is very similar to the molecule studied here) and two different exchange-correlation functionals (i.e., BLYP and B3PW91), Urakawa et al. found eleven conformers of cinchonidine by thoroughly investigating the dependence of the potential energy on the two torsion angles describing relative orientation of the quinoline and quinuclidine groups (i.e., τ_1 and τ_2 here). As shown in Table XII in the Supporting Information, a one-to-one mapping can be done between the eleven subfamilies found here and the eleven conformers previously reported.[16]

Finally, we note that the conformers in a given subfamily can be further subcategorised. Firstly, depending on the orientations of the O–CH_3 group, that is, $\tau_4 = 0^\circ$ versus $\tau_4 = 180^\circ$, we have *cis* ($\tau_4 = 180^\circ$) and *trans* ($\tau_4 = 0^\circ$) pairs with respect to the C^5–C^{11} bond.[18] In Table 1, the values of the τ_4 angle of the *cis* and *trans* conformers in a pair are highlighted in cyan and black, respectively. Secondly, depending on the orientations of the O–H bond (i.e., τ_3), the conformers in the subfamilies I, VII, IX, X and XI can be grouped into ten pairs of pseudo-conformers (see Section 3.3.3). The pseudo-conformers in a pair have very similar values for the τ_1, τ_2 and τ_4 dihedral angles and different values for τ_3, that is, positive versus negative. In Table 1, the values of the τ_3 angles of the pseudo-conformers in a given pair have the same colour, that is, either magenta or black.

3.2. Computed relative energies and Boltzmann weights

In this section, we compare the predictions made by the different sets of DFT calculations for the relative energies and the associated Boltzmann weights of the 30 conformers. The goal is to illustrate the limited character of the predictions made with DFT for these quantities. The relative energies and Boltzmann factors predicted by the six sets of calculations (see section 5) for the 30 conformers considered are compared in Figures 2–4. See Table XIII in the Supporting Information for a comparison of all computed relative energies and Boltzmann factors.

In Figure 2, the BP86, OLYP and B3LYP predictions made in both vacuum (upper panel) and COSMO (lower panel) calcula-

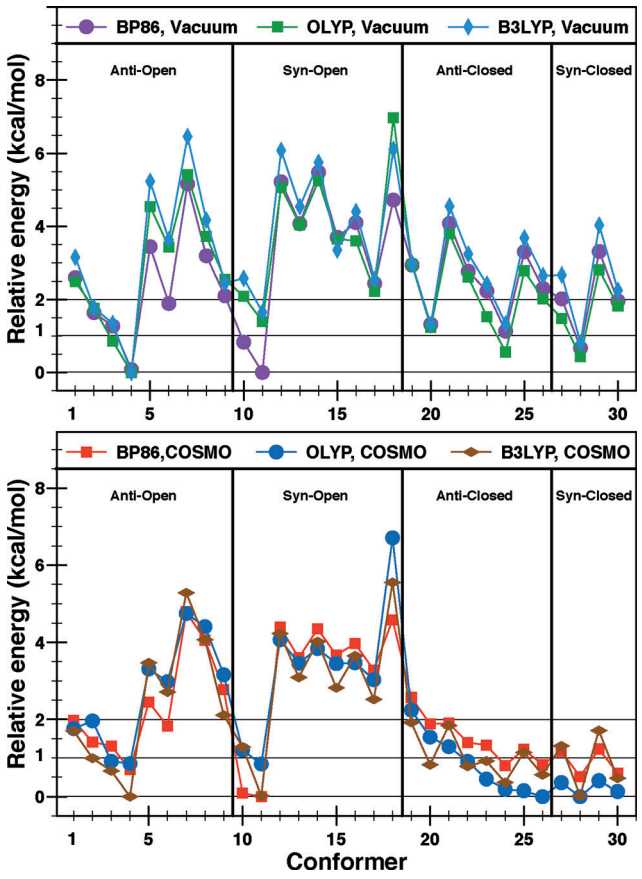

Figure 2. Dependence of the predicted relative total bonding energies of the 30 conformers on the computational parameters used in the calculations: BP86 vs. OLYP vs. B3LYP predictions in the vacuum (upper plot) and COSMO (lower plot) calculations.

tions are compared. As can be seen, the three energy plots exhibit very similar trends in both vacuum and COSMO calculations. Further, in Figure 3, we compare the vacuum and COSMO predictions made by the BP86 (upper plot), OLYP (middle plot) and B3LYP (lower plot) calculations. First, we note that the trends observed in the BP86, OLYP and B3LYP plots are again quite similar. Second, we note that there are three important changes brought about by the use of COSMO solvation model:

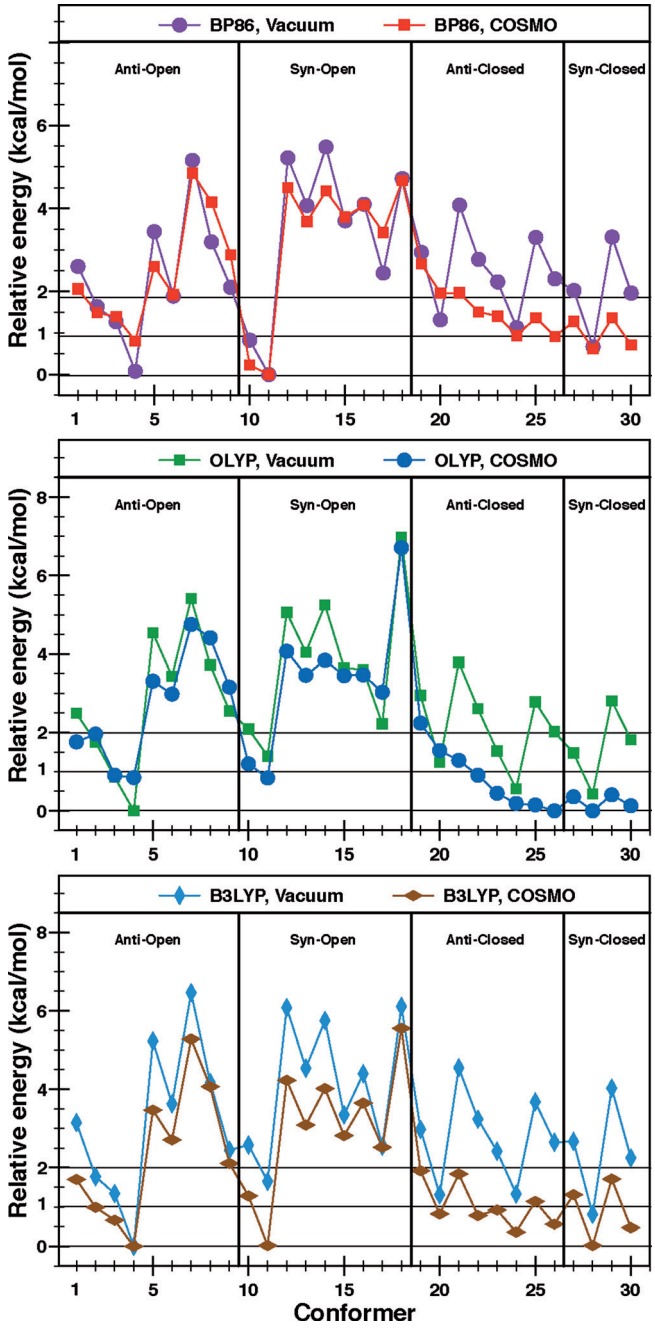

Figure 3. Dependence of the predicted relative total bonding energies of the 30 conformers on the computational parameters used in the calculations: vacuum vs. COSMO predictions in BP86 (upper plot), OLYP (middle plot) and B3LYP (lower plot) calculations.

1) A strong stabilisation of the conformers in *Anti–Closed* and *Syn–Closed* families, for example, variations of more than 2 kcal mol^{-1} in the relative energy of a given *Closed* conformer when going from vacuum to COSMO are not unusual. This observation corroborates the computational and experimental reports made in reference [13], where it was shown that polar solvents stabilise the *Closed* conformers, which are more polar.
2) A lowering of the energy gap between the conformers in a *cis–trans* pair (see Table XIV in the Supporting Information). In the vacuum calculations, the average *cis–trans* energy gaps are 1.33 (BP86), 1.11 (OLYP) and 1.58 kcal mol^{-1} (B3LYP), whereas in the COSMO calculations the average gaps are reduced to 0.59 (BP86), 0.32 (OLYP) and 0.99 kcal mol^{-1} (B3LYP). Typically, the *cis* conformers are predicted to have lower energies than their *trans* counterparts, the only exception is observed in the OLYP/COSMO calculations for conformers 1 and 2.
3) A lowering of the energy gap between the conformers in an exciton-coupling pair (see Table XV in the Supporting Information). In the vacuum calculations, the average energy gaps are 1.30 (BP86), 1.41 (OLYP) and 1.46 kcal mol^{-1} (B3LYP), whereas in the COSMO calculations the average gaps are reduced to 0.36 (BP86), 0.50 (OLYP) and 0.41 kcal mol^{-1} (B3LYP).

It is important to stress that, even though the six sets of calculations predict relative energies that exhibit similar trends and consistent changes when going from BP86 to OLYP to B3LYP or when going from vacuum to COSMO, the Boltzmann factors predicted by the six sets of calculations for the 30 conformers are very different. This is illustrated in Figure 4. As can be seen, the six sets of calculations make very different predictions, not only for the Boltzmann weights of the 30 conformers, but also for the dominant conformers.

The differences observed between the Boltzmann weights predicted at the different levels of theory are not surprising[22–25] and are a consequence of the uncertainties (at least 1–2 kcal mol^{-1}) associated with the DFT relative energies. Clearly, the individual Boltzmann factors predicted here depend too sensitively on the choice of computational parameters used (e.g., exchange-correlation functional, solvation model, basis set, etc.), and as such should be considered as rough estimations. On the other hand, the six sets of calculations make rather consistent predictions for the subfamilies expected to be predominant at room temperature. As an example, we looked at conformers 4, 11, 20, 24 and 28. The Boltzmann factors computed for these conformers (and often also for their *trans* and/or exciton-coupling counterparts) stand out among the 30 conformers irrespective of the level of theory employed. This, in spite of the fact that they differ significantly among the six sets of calculations.

We conclude this section by discussing the results obtained in reference [16] from the perspective of the results obtained in the present study. There are three important issues:

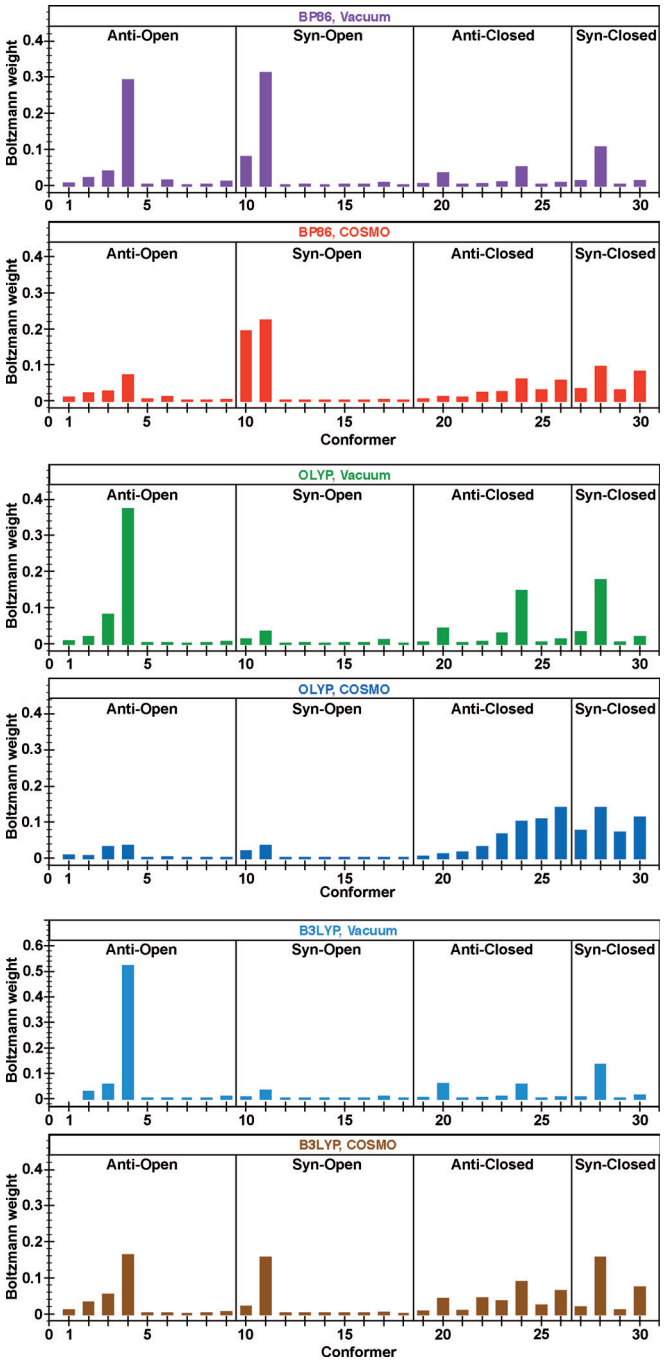

Figure 4. Comparison of the Boltzmann weights predicted by the six sets of DFT calculations.

1) The conclusions drawn here regarding the most important conformations mirror closely the conclusions drawn in reference [16]. As shown in Table XII in the Supporting Information, a one-to-one mapping can be done between the predominant conformations here (i.e., conformers 4, 11, 20, 24 and 28) and the predominant conformers in reference [16], that is, Open(3), Open(10), Closed(7), Closed(2) and Closed(1), respectively.
2) The comparison of the vacuum and COSMO Boltzmann factors in Figure 4 provides further support for the conclusion that at room temperature the population of conformer Open(3), that is, conformer 4 here, is expected to decrease in favour of the *Closed* conformers.
3) The final conclusion drawn previously regarding the Boltzmann population of conformer Open(10), that is, conformer 11 here, which exhibits an intramolecular hydrogen-bond is not supported by the comparisons of the vacuum and COSMO Boltzmann factors in Figure 4. The calculations performed here suggest that in the presence of the solvent, the population of conformer 11, that is, conformer Open(10) in ref. [16], will increase to the detriment of conformer 4, that is, conformer Open(3) in ref. [16]. Similar conclusions have also been reached on the basis of DFT-D calculations (see Table XVI in the Supporting Information). On the other hand, Urakawa et al. have concluded (by analysing the 200 K and 300 K free-energy surfaces) that the population of conformer Open(10), that is, conformer 11 here, is negligible. They acknowledged, however, that for temperatures larger than 300 K the Open(3) and Open(10) minima can merge. This will result in an increase of the population of Open(10) to the detriment of conformer Open(3).

3.3. Comparison of experimental and computed spectra

In this section, we compare the experimental VA and VCD spectra with the computed spectra. To simplify the discussion, the fingerprint interval was divided into 4 regions labelled A, B, C and D. First, the experimental spectra are compared with simulated spectra obtained as Boltzmann averages over all 30 conformations. Then, individual comparisons between the spectra computed for the most important conformers and experiment are performed. Our goal is to gain further insight regarding the predominant conformers in the experimental sample, viz., as discussed in the previous section, the Boltzmann factors predicted for the 30 conformers cannot be trusted. For brevity, only the BP86/COSMO spectra will be considered when discussing the individual comparisons. As shown in Section 3.1 in the Supporting Information, the VA and VCD spectra predicted by the BP86/Vacuum, BP86/COSMO, OLYP/Vacuum and OLYP/COSMO calculations are overall very similar, and support the conclusions drawn here based on the BP86/COSMO spectra.

3.3.1. Boltzmann-weighted fingerprint spectra

Figure 5 shows a comparison of the Boltzmann-weighted VA and VCD spectra predicted by the BP86/Vacuum, BP86/COSMO, OLYP/Vacuum and OLYP/COSMO calculations. As can be seen, all simulated VA spectra provide, qualitatively, a good agreement with the experimental VA spectra. In region D, the vacuum VA spectra reproduce the experiment better than the COSMO spectra, which provide only a qualitative agreement with the experimental spectrum. In region C, all simulated spectra exhibit weak bands as observed in the experiment as well. Further, none of the simulated spectra are able to reproduce the experimental bands observed in region B. Finally, in

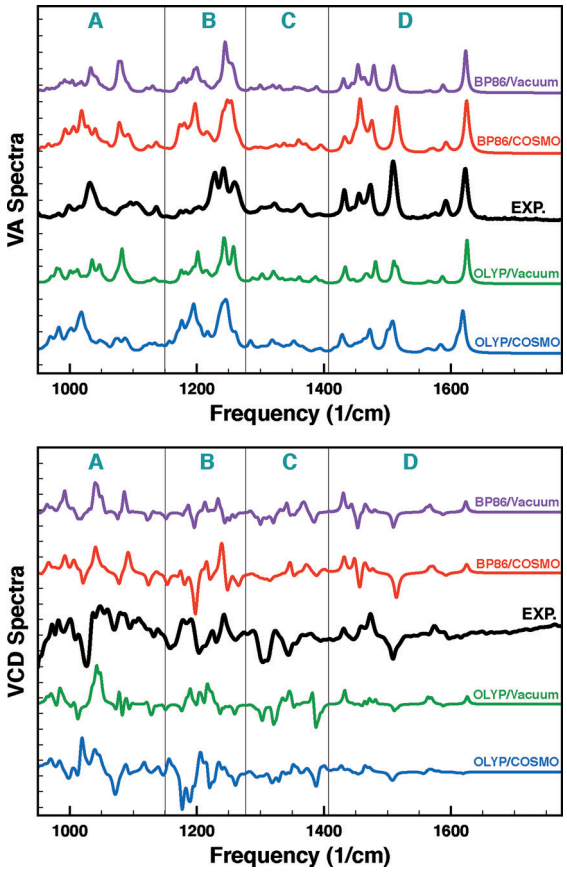

Figure 5. Fingerprint spectral region: Boltzmann-weighted VA (upper plot) and VCD (lower plot) spectra predicted by the four sets of calculations. The experimental spectra are also shown.

region A, the experimental spectrum is reproduced quite well by the OLYP/COSMO spectrum, whereas the rest of the simulated VA spectra (especially the vacuum ones) show large deviations from the experiment.

Moving to the VCD spectra, we note that the four sets of simulated VCD spectra are very different and none of them are able to reproduce the experimental spectrum. These observations suggest that the VCD spectra are significantly more sensitive to the Boltzmann factors than the VA spectra, and, more importantly, that none of the DFT calculations are able to predict the Boltzmann factors accurately. Indeed, as shown in Section 3.2 in the Supporting Information, where the simulated VA and VCD spectra of the 30 conformers are compared, the VCD spectra are significantly more sensitive to the molecular conformation than the VA spectra, that is, the VCD spectra computed for the 30 conformers exhibit very clear differences, unlike the simulated VA spectra, which are often very similar.

Consequently, to obtain insight regarding the predominant conformations in the experimental sample, we have performed individual comparisons between the spectra simulated for the 30 conformers and the experimental spectra (Section 3.2 in the Supporting Information). In the following two sections, we will discuss the most important observations made regarding these individual comparisons.

3.3.2. Conformers 4 and 11

In this section, we compare, side by side, the experimental VA and VCD spectra with the spectra computed for the conformers 4 and 11. The goal is to obtain information regarding the relative populations of these two conformers. As shown in Figure 4, some of our calculations suggest that conformer 11 should also be populated at room temperature, which appears to be in disagreement with the conclusions drawn previously.[16]

Fingerprint spectral region: Figure 6 compares the experimental VA and VCD spectra with the BP86/COSMO spectra computed for the conformers 4 and 11. As can be seen, the VA spectra of conformers 4 and 11 reproduce fairly well the experiment. In region A, the spectrum of conformer 11 reproduces the experiment marginally better than the spectrum of conformer 4. In region B, the two computed VA spectra are rather similar and provide only a qualitative description of the experimental spectrum. In region C, the spectra of conformers 4 and 11 have a complementary character with respect to the experimental spectrum, that is, the experimental bands that are missing or are too weak in one of the two computed VA spectra can be found in the other computed spectrum. In region D, the two simulated spectra reproduce fairly well the experimental spectrum, and again seem to have a complementary character.

Moving to the VCD spectra, we see that overall the VCD spectrum of conformer 4 reproduces the experimental VCD spectrum better than the spectrum of conformer 11. The VCD spectrum of conformer 4 is able to reproduce rather closely the experimental pattern in region D and also some of the intense bands in regions A and B. It is important to note, however, that in regions A and B, the VCD spectrum of conformer 4 is very nicely complemented by the spectrum of conformer 11, which exhibits some of the intense VCD bands observed in the experimental spectrum but are not in the spectrum computed for conformer 4. Further, we note that the VCD spectrum of conformer 11 provides a less accurate description of the pattern in region D than the spectrum of conformer 4, and that neither of the two computed VCD spectra are able to reproduce the experimental pattern observed in region C.

Regarding the relative populations of the conformers 4 and 11, the very intense peaks observed in the VCD spectrum of conformer 11 in region B, and the fact that the VCD spectrum of conformer 4 reproduces the experiment better than the VCD spectrum of conformer 11, suggest that the population of conformer 11 should be significantly smaller than that of conformer 4. To make an estimation of the relative populations of the two conformers, we have compared the experimental VA and VCD spectra to simulated spectra obtained as Boltzmann averaged spectra obtained by using different Boltzmann factors. As shown in Figure 6, the experimental spectrum is reasonably well reproduced when combining the spectra of conformers 4 and 11 in the ratio 0.75:0.25. We also note that variations in the Boltzmann factors of $\pm 10\%$ do not significantly change the obtained average spectra. Based on the compari-

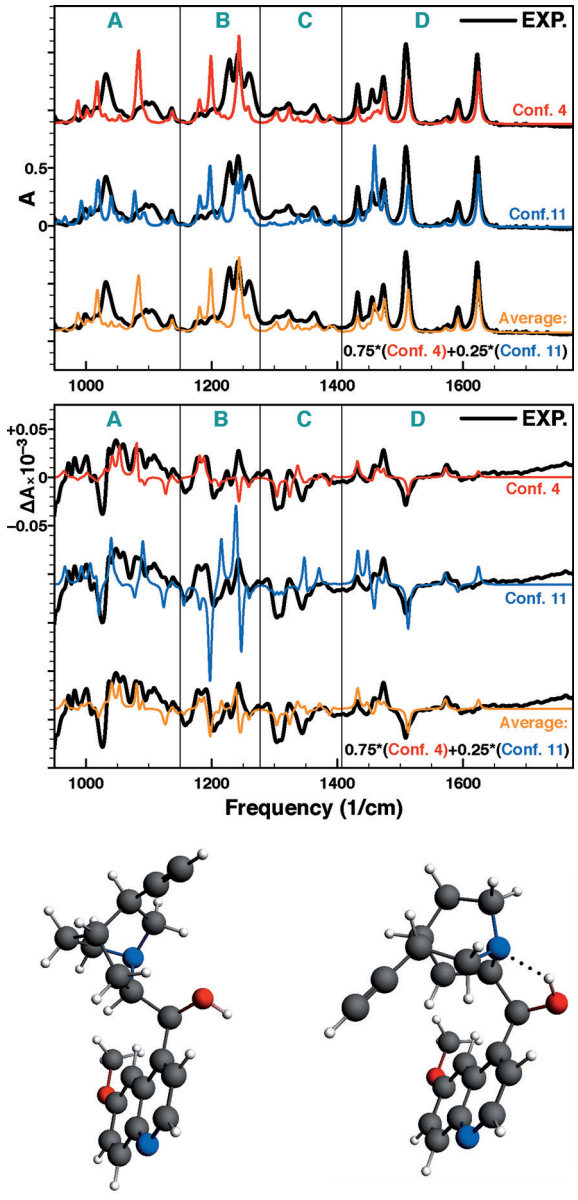

Figure 6. Fingerprint spectral region: comparison between the experimental VA and VCD spectra and the BP86/COSMO spectra of conformers 4 and 11. The simulated spectra labelled as "Average" (in orange) are obtained by Boltzmann averaging the spectra of conformers 4 and 11 by using Boltzmann factors of 0.75 and 0.25, respectively. The optimised (TZP/BP86/COSMO) structures of the conformers 4 and 11 are also shown.

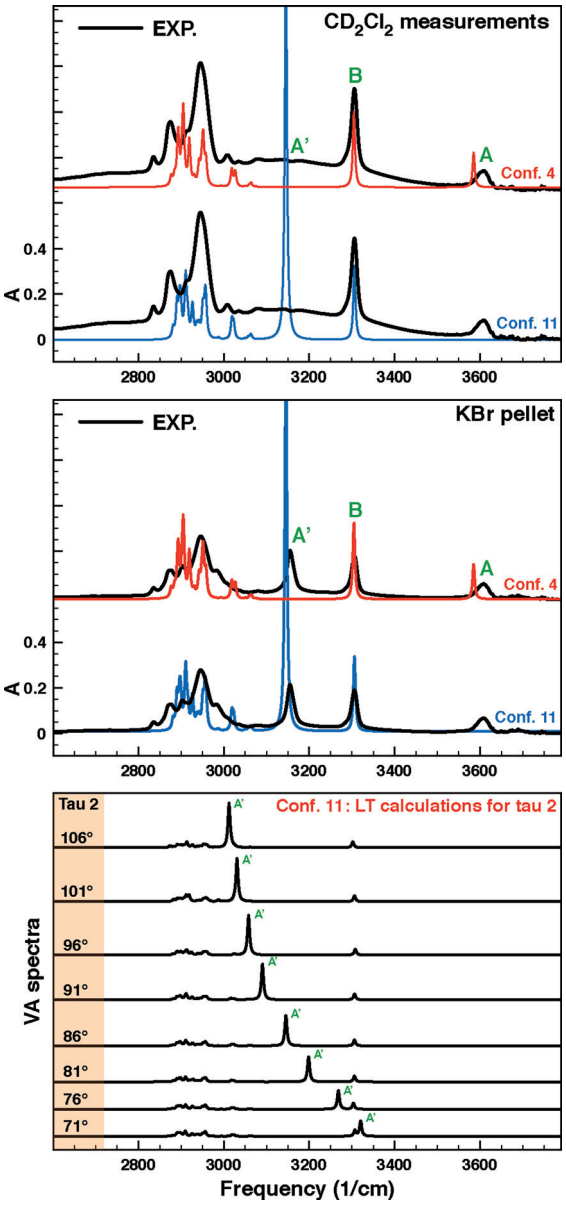

Figure 7. The 3 μm spectral region: comparison between BP86/COSMO VA spectra computed for conformers 4 and 11 and the experimental VA spectra measured in CD_2Cl_2 (upper plot) and KBr pellets (middle plot). The label A indicates the bands associated with the free O–H stretching mode, the bands labelled A′ are associated with the hydrogen-bonded O–H stretching modes (O–H···N), whereas the bands labelled as B are associated with C–H stretching modes. The lower panel shows the VA spectra computed (BP86/COSMO) for the linear transit (LT) structures, and shows how the position of the A′ band is affected by variations in the value of τ_2.

son of the fingerprint VA and VCD spectra in Figure 6, we thus conclude that conformer 4 is predominant, but it is quite likely that conformer 11 is populated at room temperature.

O–H stretching spectral region: To obtain further information on the presence of conformer 11 in the experimental sample, we have evaluated the signatures of the O–H stretching modes by extending our VA measurements into the 3 μm spectral region of the infrared spectrum. In Figure 7, we compare the VA spectra computed for the conformers 4 and 11 with experimental spectra measured in CD_2Cl_2 (upper plot) and in a KBr pellet (middle plot). We start by comparing the two VA experimental spectra. First, we note that both spectra exhibit a narrow band at 3610 cm^{-1} (labelled **A** in Figure 7), which is associated with the free O–H stretching mode. Second, we note that the CD_2Cl_2 VA spectrum exhibits a very broad underlying band around 3150 cm^{-1}, whereas the KBr pellet VA spectrum exhibits a narrow and very intense band at 3155 cm^{-1}. In Figure 7, these two bands are labelled as A and **A′** and they are both assigned to the hydrogen-bonded O–H stretching mode (O–H···N stretching modes).

Next, we looked at the O–H stretching mode in the VA spectra computed for the conformers 4 and 11. In conformer 4, the free O–H stretching mode is predicted at 3585 cm^{-1}, and as such it reproduces well the experimental bands observed around 3610 cm^{-1} in both CD_2Cl_2 and KBr pellet spectra. In conformer 11, on the other hand, the O–H stretching mode is predicted to have a frequency of 3147 cm^{-1} and a very large VA intensity (see ref. [26] for an explanation). As can be seen, this very intense band in the VA spectrum of conformer 11 is situated roughly in the middle of the broad underlying band observed in the CD_2Cl_2 experimental spectrum, and almost on top of the intense band observed at 3155 cm^{-1} in the KBr pellet spectrum.

To show that the underlying broad band observed in the CD_2Cl_2 experimental spectrum can indeed be associated with the hydrogen-bonded O–H stretching mode, we have followed the computational procedure outlined in references [19] and [20] and have perturbed the structure of conformer 11 systematically by running linear transit (LT) calculations for the τ_2 dihedral angle. During the LT scans, the τ_2 dihedral angle was varied by $\pm 20^\circ$ in steps of 5°, and the obtained LT structures were relaxed by using constrained-geometry optimisation calculations (i.e., except for the τ_2 dihedral angle, which was kept fixed, all other structural parameters were relaxed during the geometry optimisations). These partially relaxed LT structures exhibit variations in the length of the intramolecular hydrogen-bond between $\pm 10\%$ and -3% with respect to the fully relaxed structure and were all contained in an energetic window of 0.9 kcal mol^{-1}. As can be seen in the lower panel of Figure 7, these small variations in the length of the intramolecular hydrogen-bond induce very large shifts in the frequency of the O–H···N stretching mode. Consequently, we can conclude that the broad band observed in the CD_2Cl_2 experimental spectrum can indeed be associated with the O–H···N stretching mode; viz., upon Boltzmann averaging, one expects to obtain a broad underlying band. This in turn provides further evidence that at room temperature conformer 11 is present in both experimental samples. Importantly, in agreement with the conclusions drawn when analysing the fingerprint spectra, the comparison of the spectra in the O–H stretching spectral region also suggests that in the CD_2Cl_2 solution, as in the KBr pellet, the population of conformer 4 is significantly larger than that of conformer 11; viz., the very large intensity of the O–H···N stretching mode would dominate the VA spectra otherwise. Finally, we note that additional measurements in DMSO may indirectly provide further evidence for the occurrence of intramolecular hydrogen-bonding in the experimental sample as the VA and VCD bands associated with intramolecular hydrogen-bonding are expected to be suppressed in DMSO.

3.3.3. Large-amplitude motions

The large changes observed in the VA spectra computed for the linear transit structures of conformer 11 (Figure 7) prompted us to investigate closer the effects induced in the VA and VCD spectra by large-amplitude motions. As the barrier required to rotate the hydroxyl group around the C^{11}–O^{22} bond is expected to be very small, we have systematically varied the orientation of the O^{22}–H^{44} bond by performing τ_3 LT calculations. During the LT scans, the τ_3 dihedral angle was rotated over 360° in steps of 20°. The LT calculations have been performed by using the BP86 functional and the COSMO solvation models. Only the conformers in the subfamilies predicted to be dominant at the BP86/COSMO level of theory have been considered, that is, the conformers in the subfamilies I, V, IX, X and XI (Figure 4).

Figure 8 shows the variation of the energy during the LT scans performed for the *cis* conformers 4, 11, 20, 24 and 28 (the case of the *trans* conformers, which have slightly higher energies, will not be discussed as it is very similar to the *cis* situation. The *cis* and *trans* LT energy curves are compared in Figure S8 in the Supporting Information). Conformer 11 is the only conformer exhibiting a high rotational barrier, that is, 5.3 kcal mol^{-1}. Given the fact that in this conformer the hydroxyl group is involved in an intramolecular hydrogen-bond with the N atom number 24, this is not surprising. For the rest of the conformers, the rotational barrier is very small. In conformers 24 and 28, variations of 140° in τ_3 induce almost no change in energy. The relative energy and the energy barrier between conformers 28 and 30 are 0.09 and 0.45 kcal mol^{-1}, respectively, whereas in the case of conformers 22 and 24, the relative energy and the rotational barrier are both 0.6 kcal mol^{-1}. Clearly, the conformers that differ only in the orientation of the hydroxyl group cannot be considered as genuinely different conformers—pseudo-conformers would be a more appropriate nomenclature for them. Further, we note that additional complications are found when looking at the energy curves of conformers 4 and 26, which exhibit somewhat higher rotation barriers, that is, between 1.4 and 1.94 kcal mol^{-1}. In the case of conformer 4, the LT calculations reveal a local minimum that was not found during the conformational search, whereas in the case of conformer 26, the end point of the 360° LT scan for τ_3 is not conformer 26 but conformer 22. Clearly, we are dealing with an extremely complicated situation that cannot be described by considering the conformers obtained from a standard conformational analysis. In an attempt to account for this complicated potential energy surface (PES) in a simulation, VA and VCD calculations were performed for all τ_3 LT structures situated within an energetic window of 1 kcal mol^{-1} and in the vicinity of a local minimum associated with conformers 4, 24, 26 and 28. Because of the high barrier, no VA and VCD calculations were performed for the τ_3 LT structures associated with conformer 11.

The τ_3 LT spectra associated with each conformer have been Boltzmann-averaged separately and the results are shown in Figure 9. For comparison, the experimental VA and VCD spectra, and spectra computed for the relaxed structure of conformer 11 are also shown in Figure 9. As can be seen, all five simulated VA spectra reproduce the experiment decently—none of them stand out as significantly better or worse than the other. In the case of the VCD spectra, the differences are more pronounced. For example, the Boltzmann spectra associated with conformers 24 and 26 can be immediately discarded. The

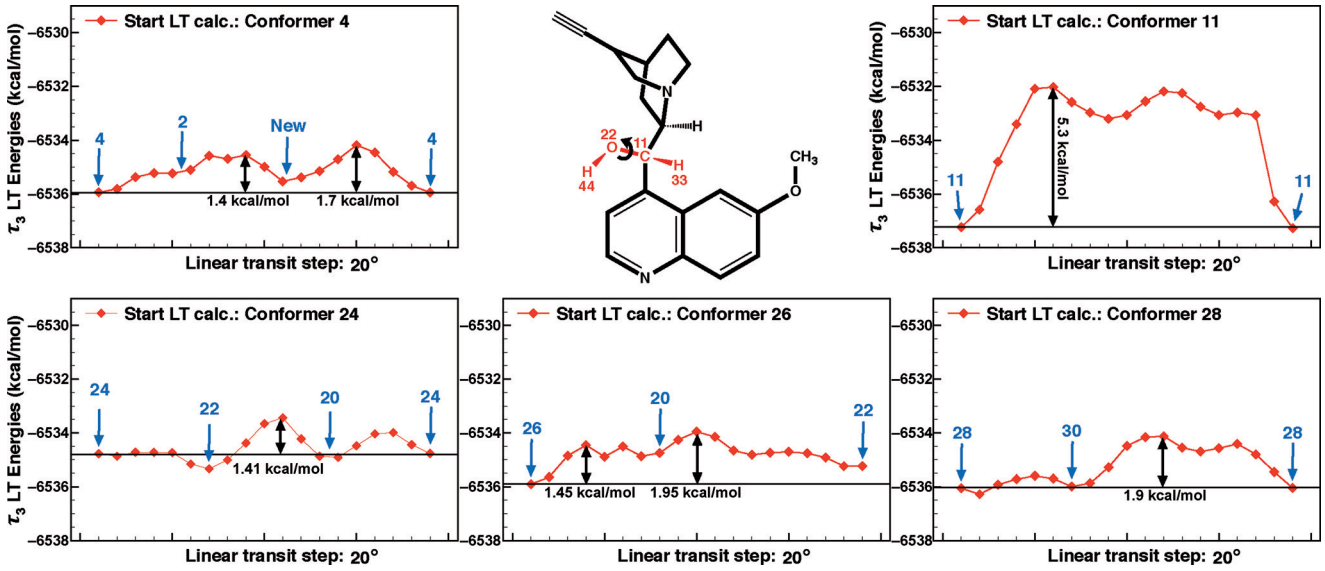

Figure 8. Variation of the energy of conformers 4, 11, 20, 24 and 28 during linear transit scans for τ_4. The τ_4 angle is varied through 360° in steps of 20°. The same energy window is shown in all plots.

spectrum of 24 has opposite signs with respect to the experiment in region D, whereas spectrum of 26 exhibits very intense VCD bands in region B that are not seen in the experiment. Further, we note that the experimental pattern in region D is reproduced rather closely by the Boltzmann-weighted spectrum of conformer 4. Unfortunately, this is the only situation in which a clear agreement between calculation and experiment is obtained. The spectrum of conformer 4 also manages to reproduce some of the experimental patterns seen in region A, but is unable to reproduce the experimental features seen in regions B and C. However, the spectra associated with conformers 11 and 28 seem to exhibit the patterns seen in the experimental spectrum in region B, and as such one can assume that they complement the spectrum of conformer 4 (see also the discussion in Section 3.3.2).

We conclude this section by noting that the comparison of the spectra in Figure 9 have further reinforced the conclusion drawn in Section 3.3.2, namely, that conformer 4 is the dominant conformer. Regarding the discrepancies observed between calculation and experiment, the analysis of the LT energy curves in Figure 8 shows clearly that the discrepancies can be traced back to the inability to perform a proper vibrational average for DHQD using the computational methods presently available. Finally, we note that, as will be discussed in the next section, the characteristics exhibited by the VCD spectra of the pseudo-conformers make the need to perform a rigorous vibrational average of the spectra even more critical.

3.3.4. Exciton coupling

Our goal in this section is to show that the presence/absence of the VCD exciton bands in the simulated and/or experimental VCD spectra provides important insights into the conformational dynamics occurring in the experimental sample. We start by noting that among the 30 conformers considered, there are ten pairs of pseudo-conformers, that is, (1,3), (2,4), (14,16), (15,17), (19,21), (20,22), (23,25), (24,26), (27,29) and (28,30). As discussed in the previous section, and as can be seen in Table 1, the structures of the pseudo-conformers in a pair differ mostly in the orientation of the hydroxyl group. For brevity but without loss of generality, we will discuss here the structures and spectra of only one pair of pseudo-conformers, that is, conformers 28 and 30. We have considered this pair because conformer 28 was predicted by all six set of calculations as the most important *Closed* conformer.

Figure 10 shows comparisons of the structures and VCD spectra simulated for conformers 28 and 30. As highlighted, the two conformers differ only in the orientation of the O–H bond (i.e., in τ_3). This small structural difference, however, induces very significant effects in the VCD spectra (and only minor changes in the VA spectra). As can be seen, in region B, the VCD spectrum of conformer 30 exhibits bands that are 3–4 times more intense than the bands in the VCD spectrum of conformer 28. Because these intense VCD bands are not seen in the experimental spectrum, one might be tempted to conclude that conformer 30 is not present in the experimental sample. A similar conclusion would be reached as well for conformer 28, the VCD spectrum of which does not reproduce the experimental one particularly well. In contrast to this, a reasonable agreement between the experimental and the simulated VCD spectrum is obtained by averaging the LT structures around the local minima associated with conformers 28 and 30. This indicates that conformers 28 and 30 may very well be present in the experimental sample at room temperature—a conclusion that would not be reached based on the spectra computed for the individual conformers. As the situation described here for conformers 28 and 30 is also found when looking at other pseudo-conformers, it should be clear that vi-

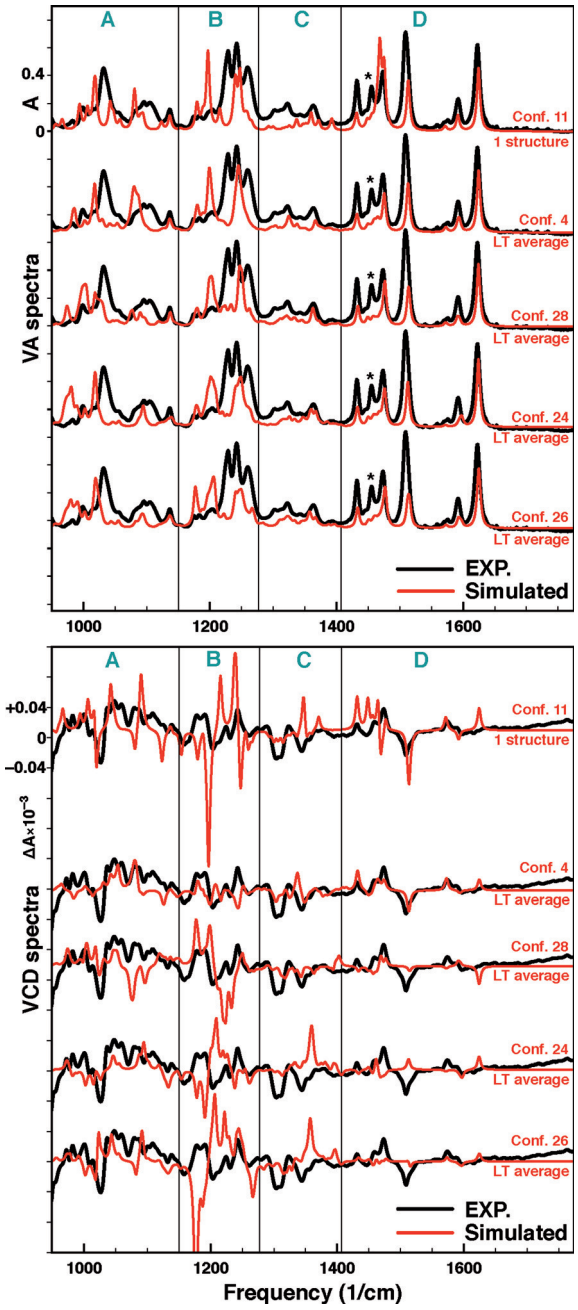

Figure 9. Comparison of experimental VA and VCD spectra and simulated (BP86/COSMO) spectra obtained by Boltzmann averaging the spectra computed for the τ_3 linear transit structures of conformers 4, 24, 26 and 28 within an energetic window of 1 kcal mol^{-1}. The spectra computed for the relaxed structure of conformer 11 are also shown. The experimental VA band highlighted with a star is characteristic of *trans* conformers and, as such, is not reproduced by the spectra of the *cis* conformers considered here.

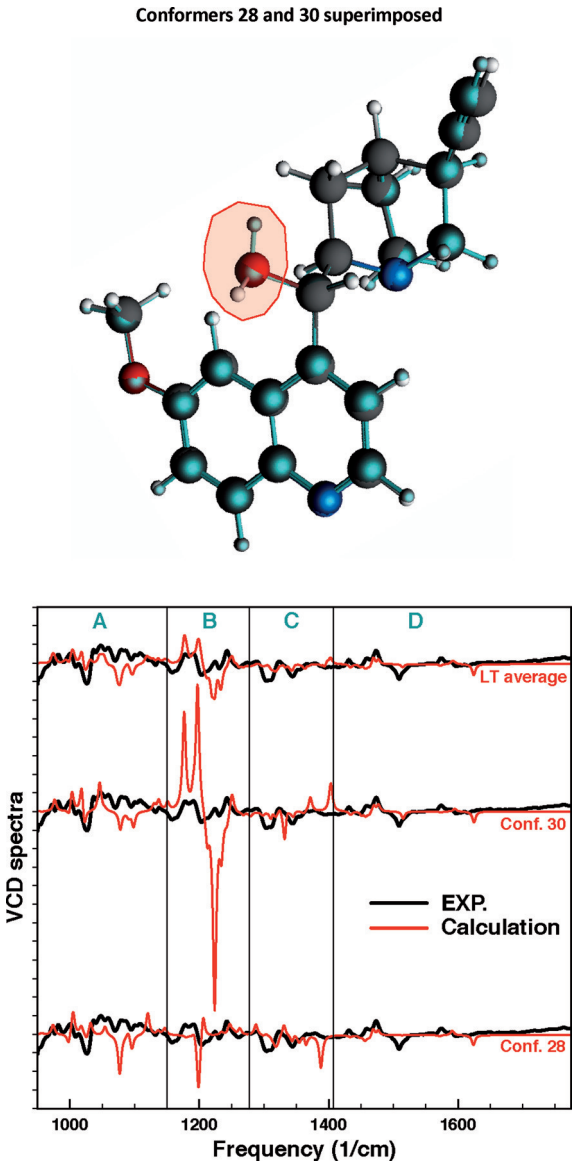

Figure 10. Comparison of the BP86/COSMO structures and VCD spectra of conformers 28 and 30. The experimental VCD spectra, and the simulated spectra obtained as Boltzmann averages of the VCD spectra computed for the τ_3 LT structures in the vicinity of the minima associated with conformers 28 and 30 and within an energetic window of 1 kcal mol^{-1} are also shown. Regarding the superimposed structures, we note that all atoms of conformer 28 have been highlighted in green. Depending on the viewing angle, however, some atoms in green cannot be seen as they are blocked by the equivalent atoms of molecule 30.

brational averaging cannot be neglected in the case of the pseudo-conformers as it significantly changes the appearance of the simulated VCD spectra.

Regarding the intense VCD signals observed in region B of conformer 30, we note that they can be explained by using the VCD exciton-coupling (EC) model.[27,28] As shown in Section 5 in the Supporting Information, the very intense VCD bands are attributed to the coupling between the electric dipole transition moments associated with the O^{22}–H^{44} and C^{2}–O^{21} polar bonds. It is worth noting the atypical and thus very interesting character of these EC VCD bands, which are observed around 1200 cm^{-1} and are associated with modes involving C–H and O–H bending movements; viz., the typically EC VCD bands are associated with carbonyl stretching modes and are observed around 1700 cm^{-1}. We note that other studies[28,29] have also reported similar observations and have proposed the use of the EC VCD model for the interpretation of VCD bands that are not associated with carbonyl stretching modes. We stress, however, that we have used the EC VCD

model as an enhancement mechanism to explain the very intense VCD signals observed in the spectra of some of the pseudo-conformers. We do not support the use of the EC VCD model as an alternative to DFT calculations for determining the absolute configuration of chiral molecules.

We conclude by saying that the calculations performed in this section show that when considering the VCD spectra of DHQD, the experimental situation cannot be simulated by simply Boltzmann averaging the spectra computed for the conformers predicted by a standard conformational search. The reason is threefold: 1) the large differences between the VCD spectra of the pseudo-conformers in a given pair (see Figures S5–S7 in the Supporting Information), 2) the small energy barriers between the pseudo-conformers in a pair, and 3) the large uncertainties in the predicted Boltzmann factors. As shown in Figure 10, the VCD simulated spectrum obtained by Boltzmann averaging the VCD spectra of the LT structures situated in the vicinity (i.e., within an energetic window of 1 kcal mol^{-1}) of the minima associated with the conformers 28 and 30 reproduces the experimental VCD spectrum fairly well. This demonstrates the need to perform a vibrational average of the VCD spectra in this case—especially as the situation encountered above for the conformers 28 and 30 (i.e., small energy barriers, small relative energies and very different VCD spectra) is also common in other pairs of pseudo-conformers (see Figures S5–S8 in the Supporting Information).

4. Conclusion

By using the experimental VA and VCD spectra of the dehydroquinidine (DHQD) molecule as a reference, we have performed a very thorough analysis of the predictions made by the various DFT methods for the structures, VA spectra, VCD spectra and Boltzmann populations of the most important conformers of this molecule. To this end, we have performed vacuum and COSMO DFT calculations by using three different exchange-correlation functionals, that is, BP86, OLYP and B3LYP. The six sets of DFT calculations performed predicted very similar structures, but very different Boltzmann factors for the 30 considered conformers of DHQD. As a result, the simulated VCD spectrum (obtained as Boltzmann averages over the spectra of the considered conformers) depends sensitively on the computational parameters used.

Individual comparisons between the experimental VA and VCD spectra and the spectra computed for the 30 conformers have shown that conformer 4, that is, the so-called Open(3) conformer, is the dominant conformer in the experimental sample. This is in agreement with previous findings. To gain insight regarding the populations of the rest of the conformers, we have analysed with respect to the experimental spectra the relative magnitude of a few key marker bands in the VA and VCD spectra computed for the 30 conformers considered. First, we evaluated the VA bands associated with the O–H stretching bonds. As discussed in Section 3.3.2, the presence of a very broad underlying band centred around 3150 cm^{-1} provides evidence that conformers exhibiting intramolecular hydrogen-bonding, for example, conformer 11, are present in a small percentage in the experimental sample at room temperature. Second, we investigated the exciton-coupling VCD bands observed in the VCD spectra of 10 conformers (see Section 3.3.4). To explain the lack of VCD exciton-coupling bands in the experimental spectrum, we closely analysed the structural differences between the pseudo-conformers in a pair by performing linear transit calculations for the dihedral angle giving the orientation of the hydroxyl group at the chiral centre, that is, an additional degree of freedom in the conformational space of the cinchona alkaloid previously unexplored at the DFT level of theory. This investigation has shown that in the pseudo-conformers, the O–H bond is likely to execute slow movements with large amplitude, and that these large-amplitude motions trigger the appearance/disappearance of the strong exciton-coupling VCD bands. This has important implications. On one hand, it suggests that VCD can be employed for studying intramolecular relaxation phenomena such as low-frequency and large-amplitude motions. On the other hand, it provides additional evidence[19–21] that, when studying flexible molecules with polar bonds, the vibrational averaging of VCD spectra should not be neglected. As, in this regard, the dehydroquinidine molecule considered here is expected to be a typical example, that is, not the exception to the rule. This strong interplay between exciton coupling and large-amplitude-motion phenomena further underscores the need for computational tools capable of performing rigorous vibrational averaging of the VCD spectra over the harmonic oscillator wave function.

5. Experimental and Computational Details

5.1. Experimental details

The DHQD molecule was synthesised in the bio-organic synthesis group at the University of Amsterdam.[30] Fourier-transform infrared (FTIR) and VCD spectra were obtained by using a Bruker Vertex 70 spectrometer in combination with a PMA 50 module for polarisation modulation measurements. The PEM centre frequency was set to 1500 cm^{-1} for all the measurements in the fingerprint region. Samples were prepared in CD_2Cl_2 and kept in sealed infrared cells with 3 mm thick CaF_2 windows. Baseline correction was performed by using the spectrum of dry CD_2Cl_2. Similar measurements have been attempted using acetonitrile as the solvent, but because of the relatively low solubility, these VCD spectra could not reliably be used for further analysis. KBr pellets were prepared with a mixture of KBr/DHQD in a ratio of about 100:1.

5.2. Computational details

The conformational space of DHQD was explored in two steps. First, a molecular mechanics (MM) conformational search was performed, then the MM conformers were further re-optimised by using density functional theory (DFT). The MM conformational search was done with the Macromodel v9.7 program using the MM3 force field,[31] the GBSA solvent model for chloroform and a 10 kcal mol^{-1} energy cut-off window.

All DFT calculations (i.e., geometry optimisation[32], VA[33] and VCD[34] calculations) were performed with the ADF program package.[35–37] Both vacuum and COSMO[38–40] calculations were performed by using the ADF TZP[41] basis set and three different exchange-correlation functionals (BP86,[42,43] OLYP[44,45] and B3LYP[46,47]). In the vacuum calculations, all geometry optimisations, VA and VCD calculations were performed for the isolated conformers, whereas in the COSMO calculations the considered conformers were embedded in the dielectric continuum corresponding to dichloromethane, that is, dielectric constant of 8.9. Stringent convergence criteria were used in all geometry optimisations calculations, that is, 10^{-4} Hartree/Angstrom for gradients.

The VA and VCD spectra have not been computed by using the B3LYP functional. The reason is threefold. First, because Slater-type orbitals are used as basis functions in ADF and, as such, all matrix elements are calculated numerically, frequency calculations using hybrid exchange-correlation functionals like B3LYP are extremely expensive. Second, as shown,[20,34,48–50] the VCD (also VA) spectra computed by using the BP86 and OLYP functionals reproduce the experimental spectra as well as those computed by using B3LYP. Third, the VA and VCD spectra computed for DHQD at the BP86 and OLYP levels of theory are overall rather similar to the B3LYP spectra computed in reference [18] (see Figure 10) for the quinidine molecule (which structurally is very similar to DHQD).

The calculated IR and VCD spectra were obtained by Lorentzian broadening of the dipole and rotational strengths using a half-width of 8 cm^{-1}. The computed harmonic frequencies have been scaled with factors of 1.015 in the fingerprint region and 0.985 in the 3_μm region. These values were found to provide the best agreement between the experimental and computed VA and VCD bands. The analysis of the normal modes and VA and VCD spectra was performed by using the ToolsVCD program.[51]

Acknowledgements

This work was supported by The Netherlands Organization for Scientific Research (NWO).

Keywords: alkaloids · IR spectroscopy · organocatalysis · quantum chemistry · vibrational circular dichroism

[1] N. Maeda, K. Hungerbuhler, A. Baiker, *J. Am. Chem. Soc.* **2011**, *133*, 19567 – 19569.
[2] E. Schmidt, T. Mallat, A. Baiker, *J. Catal.* **2010**, *272*, 140 – 150.
[3] E. Schmidt, C. Bucher, G. Santarossa, T. Mallat, R. Gilmour, A. Baiker, *J. Catal.* **2012**, *289*, 238 – 248.
[4] J. Wang, W. Wang, W. Li, X. Hu, K. Shen, C. Tan, X. Liu, X., *Chem. Eur. J.* **2009**, *15*, 11642 – 11659.
[5] I. Motorina, C. M. Crudden, *Org. Lett.* **2001**, *3*, 2325 – 2328.
[6] L. Jiang, Y.-C. Chen, *Catal. Sci. Technol.* **2011**, *1*, 354 – 365.
[7] W. Qin, A. Vozza, A. M. Brouwer, *J. Phys. Chem. C* **2009**, *113*, 11790 – 11795.
[8] T. Kumpulainen, A. M. Brouwer, *Phys. Chem. Chem. Phys.* **2012**, *14*, 13019 – 13026.
[9] G. D. H. Dijkstra, R. M. Kellogg, H. Wynberg, J. S. Svendsen, I. Marko, K. B. Sharpless, *J. Am. Chem. Soc.* **1989**, *111*, 8069 – 8076.
[10] G. D. H. Dijkstra, R. M. Kellogg, H. Wynberg, *J. Org. Chem.* **1990**, *55*, 6121 – 6131.
[11] M. Aune, A. Gogoll, O. Matsson, *J. Org. Chem.* **1995**, *60*, 1356 – 1364.
[12] U. Berg, M. Aune, O. Matsson, *Tetrahedron Lett.* **1995**, *36*, 2137 – 2140.
[13] T. Bürgi, A. Baiker, *J. Am. Chem. Soc.* **1998**, *120*, 12920 – 12926.
[14] T. Bürgi, A. Vargas, A. Baiker, *J. Chem. Soc. Perkin Trans. 2* **2002**, 1596 – 1601.
[15] A. Vargas, N. Bonalumi, D. Ferri, A. Baiker, *J. Phys. Chem. A* **2006**, *110*, 1118 – 1127.
[16] A. Urakawa, D. M. Meier, H. Rüegger, A. Baiker, *J. Phys. Chem. A* **2008**, *112*, 7250 – 7255.
[17] T. Marcelli, *WIREs Comput. Mol. Sci.* **2011**, *1*, 142 – 152.
[18] A. Sen, A. Bouchet, V. Lepére, K. LeBarbu-Debus, D. Scuderi, F. Piuzzi, A. Zehnacker-Rentien, *J. Phys. Chem. A* **2012**, *116*, 8334 – 8344.
[19] M. Heshmat, E. J. Baerends, P. L. Polavarapu, V. P. Nicu, *J. Phys. Chem. A* **2014**, *118*, 4766 – 4777.
[20] M. Passarello, S. Abbate, G. Longhi, S. Lepri, R. Ruzziconi, V. P. Nicu, *J. Phys. Chem. A* **2014**, *118*, 4339 – 4350.
[21] J. Kapitán, C. Johannessen, P. Bour, L. Hecht, L. D. Barron, *Chirality* **2009**, *21*, S4 – S12.
[22] S. Grimme, *Angew. Chem. Int. Ed.* **2006**, *45*, 4460 – 4464; *Angew. Chem.* **2006**, *118*, 4571 – 4575.
[23] P. R. Schreiner, A. A. Fokin, R. A. Pascal, A. de Meijere, *Org. Lett.* **2006**, *8*, 3635 – 3638.
[24] M. D. Wodrich, C. Corminboeuf, P. von Ragué Schleyer, *Org. Lett.* **2006**, *8*, 3631 – 3634.
[25] T. Andras Rokob, A. Hamza, I. Papai, *Org. Lett.* **2007**, *9*, 4279 – 4282.
[26] V. P. Nicu, J. Autschbach, E. J. Baerends, *Phys. Chem. Chem. Phys.* **2009**, *11*, 1526 – 1538.
[27] G. Holzwarth, I. Chabay, *J. Chem. Phys.* **1972**, *57*, 1632 – 1635.
[28] T. Taniguchi, K. Monde, *J. Am. Chem. Soc.* **2012**, *134*, 3695 – 3698.
[29] S. Abbate, G. Mazzeo, S. Meneghini, G. Longhi, S. E. Boiadjiev, D. A. Lightner, *J. Phys. Chem. A* **2015**, *119*, 4261 – 4267.
[30] T. Marcelli, *Cinchona-derived organocatalysts for asymmetric carbon–carbon bond formation*, PhD Thesis, University of Amsterdam, Amsterdam, **2006**.
[31] Schrödinger llc, **2009**, http://www.schrodinger.com.
[32] M. Swart, F. M. Bickelhaupt, *J. Comput. Chem.* **2008**, *29*, 724 – 734.
[33] S. K. Wolff, *Int. J. Quantum Chem.* **2005**, *104*, 645 – 659.
[34] V. P. Nicu, J. Neugebauer, S. K. Wol, E. J. Baerends, *Theor. Chem. Acc.* **2008**, *119*, 245 – 263.
[35] Amsterdam density functional program, http://www.scm.com.
[36] G. te Velde, F. M. Bickelhaupt, E. J. Baerends, C. Fonseca Guerra, S. J. A. van Gisbergen, J. G. Snijders, T. Ziegler, *J. Comput. Chem.* **2001**, *22*, 931 – 967.
[37] C. Fonseca Guerra, J. G. Snijders, G. te Velde, E. J. Baerends, *Theor. Chem. Acc.* **1998**, *99*, 391 – 403.
[38] A. Klamt, G. Schürmann, *J. Chem. Soc. Perkin Trans. 2* **1993**, 799 – 805.
[39] A. Klamt, *J. Phys. Chem.* **1995**, *99*, 2224 – 2235.
[40] A. Klamt, V. Jones, *J. Chem. Phys.* **1996**, *105*, 9972 – 9981.
[41] E. van Lenthe, E. J. Baerends, *J. Comput. Chem.* **2003**, *24*, 1142 – 1156.
[42] J. P. Perdew, *Phys. Rev. B* **1986**, *33*, 8822 – 8824.
[43] A. D. Becke, *Phys. Rev. A* **1988**, *38*, 3098 – 3100.
[44] N. C. Handy, A. J. Cohen, *Mol. Phys.* **2001**, *99*, 403 – 412.
[45] F. A. Hamprecht, A. J. Cohen, N. C. Handy, *J. Chem. Phys.* **1998**, *109*, 6264 – 6271.
[46] A. D. Becke, *J. Chem. Phys.* **1993**, *98*, 5648 – 5652.
[47] P. J. Stephens, F. J. Devlin, C. F. Chabalowski, M. J. Frisch, *J. Phys. Chem.* **1994**, *98*, 11623 – 11627.
[48] V. P. Nicu, E. J. Baerends, *Phys. Chem. Chem. Phys.* **2009**, *11*, 6107 – 6118.
[49] V. P. Nicu, E. Debie, W. Herrebout, B. Van Der Veken, P. Bultinck, E. J. Baerends, *Chirality* **2009**, *21*, E287 – E297.
[50] V. P. Nicu, M. Heshmat, E. J. Baerends, *Phys. Chem. Chem. Phys.* **2011**, *13*, 8811 – 8825.
[51] V. P. Nicu, J. Neugebauer, E. J. Baerends, *J. Phys. Chem. A* **2008**, *112*, 6978 – 6991.

Received: August 17, 2015
Published online on November 27, 2015